Unraveling the Pathways of Tribochemical Reactions Involving the ZDDP Lubricant Additive by Machine-Learning-Informed Molecular Dynamics

Enrico Pedretti[1], Francesca Benini[1], Giovanni Gravili[1], and Maria Clelia Righi[1]*
[1]*Physics and Astronomy Department, University of Bologna, Viale Berti Pichat 6/2, 40127, Bologna (Italy)*

Zinc dialkyldithiophosphate (ZDDP) remains one of the most effective antiwear additives, yet the tribochemical mechanisms leading to its characteristic tribofilm formation have been debated for over 80 years. A molecular-level understanding of these reactions is crucial for designing environmentally friendly alternatives with comparable performance. Although experimental studies have identified the main constituents of the ZDDP tribofilm—namely FeS and a glassy Zn/Fe polyphosphate network—the mechanistic details of its formation remain incomplete. Computational simulations offer a unique means to probe these buried interface phenomena; however, density functional theory (DFT) provides the required chemical accuracy only at prohibitive computational cost, while conventional molecular dynamics (MD) lacks the necessary fidelity. To address this challenge, we developed the first Machine Learning Potential (MLP) specifically tailored for modeling ZDDP tribofilm formation. Using this MLP, we investigated film growth on Fe interfaces of varying reactivity, including Fe(110), Fe(210), Fe surfaces with asperities, and oxidized Fe. Our results reveal that the formation of linkage isomers through alkyl-chain transfer—described as S-to-O substitution within the molecule—is a key step in generating the polyphosphate networks characteristic of ZDDP-derived tribofilms. These simulations provide the first comprehensive, atomistically resolved picture of the dynamic processes governing ZDDP tribofilm formation.

I. INTRODUCTION

For nearly eight decades, Zinc Dialkyldithiophosphates (ZDDPs) have played a pivotal role as lubricant additives in both industrial and automotive applications. These molecules feature a reactive core composed of zinc, phosphorus, sulfur, and oxygen, with varying alkyl chains. Their effectiveness arises from the formation of a protective tribofilm under high temperature and extreme tribological conditions, a process that remains a subject of continuing debate within the tribology community[1]. However, concerns about ZDDP's environmental impact are increasing, as its decomposition products can degrade catalytic converters in vehicle exhaust systems and contribute to harmful emissions[2, 3]. A deeper understanding of tribofilm formation could therefore enable the design of alternative additives with a lower environmental footprint while maintaining or even enhancing performance.

Structurally, ZDDP-derived tribofilms comprise a sulfur-rich interfacial layer covered by zinc and iron phosphate compounds. The phosphate layer exhibits a compositional gradient, with short-chain phosphates near the substrate and longer-chain polyphosphates closer to the surface. Continuous rubbing leads to phosphate chain shortening, which strengthens the film and improves wear resistance[4]. Despite extensive investigation, the complex sequence of chemical and mechanical steps that drive tribofilm growth remains only partially understood. Current models suggest a multi-step mechanism involving[1, 5]: (i) adsorption of ZDDP molecules on ferrous surfaces via sulfur atoms; (ii) formation of iron and zinc sulfide or sulfate species; (iii) alkyl transfer reactions between oxygen and sulfur atoms, leading to linkage isomer intermediates; (iv) polymerization of phosphate units into zinc and iron polyphosphates; and (v) gradual depolymerization and reorganization during sliding.

As highlighted by Spikes in his recent review, which summarizes two decades of research on ZDDP, several key questions remain open[1]. These include: (i) the detailed reaction mechanism leading from adsorbed ZDDP to the initial sulfide layer, (ii) the molecular pathways governing phosphate network formation, (iii) the chemical and mechanical routes leading to film removal, and (iv) whether the transfer of alkyl groups from oxygen to sulfur, forming the di(thioalkyl)phosphate linkage isomer, plays a key role in driving tribofilm formation.

While experimental approaches have provided important insights, probing these atomic-scale mechanisms in situ remains challenging. Computational methods such as *ab initio* and reactive molecular dynamics simulations have clarified the early adsorption, decomposition and sulfur elimination steps, as well as providing evidence for alkyl transfer, olefin elimination, and phosphate polymerization[6–11]. However, these approaches are either computationally expensive or unable to accurately capture bond formation and breaking at tribological timescales. Consequently, a predictive atomistic picture of tribofilm growth is still lacking.

Another factor that significantly influences tribofilm formation is the reactivity of the substrate. Surface composition, crystallographic orientation, and oxidation determine how ZDDP molecules adsorb, decompose, and react to form the initial sulfide layer[8, 9]. Similarly, the

* clelia.righi@unibo.it

different surface energies of Fe(110) and Fe(210) facets can alter adsorption energies and reaction barriers, influencing both the nucleation rate and the chemical composition of the resulting film. These effects are crucial for understanding how tribofilms develop under realistic conditions, where surface roughness and oxidation dynamically evolve during sliding.

A promising concept is that linkage isomers, alternative molecular forms of ZDDP obtained via S-to-O substitution, may play a central role in tribochemical reactivity[6, 7, 12]. These isomers, denoted LI1-ZDDP and LI2-ZDDP (one and two S-to-O substitutions, respectively), are more stable than the parent ZDDP molecule and they display distinct dissociation pathways and bonding patterns under load. Our calculations demonstrated that such isomerization stabilizes phosphate and phosphite groups, suggesting a potential influence on tribofilm nucleation and growth[12].

Building on these insights, the present study combines density functional theory (DFT) calculations and machine learning molecular dynamics (ML-MD) simulations to investigate ZDDP and its linkage isomer LI2-ZDDP confined between Fe interfaces under realistic tribological conditions of load, temperature, and sliding. Machine Learning Potentials are developed through our Smart Configuration Sampling (SCS) active-learning protocol[13], which is specifically designed for tribology, and employs an iterative process to produce a complete DFT dataset (and train a potential) that captures the wide variety of tribological phenomena for the chosen system and conditions. This approach enables chemically accurate yet computationally efficient simulations of tribochemical reactions at scales significantly larger than those accessible by *ab initio* methods. By comparing ZDDP with its LI2-ZDDP linkage isomer across Fe interfaces of different reactivity (Fe(210), Fe(110), and oxidized surfaces), we directly explore how molecular isomerization and substrate reactivity affect tribofilm formation mechanisms and polyphosphate growth rates, thereby addressing several outstanding questions identified in the literature.

II. METHODS

A. MLP training

This work employs two machine learning potential (MLP) architectures: MACE [14][15], selected for its excellent accuracy (at the price of higher computational cost), and DeePMD-kit [16] (with the *se_e2_a* descriptor), whose high computational efficiency makes it particularly suitable for large-scale molecular dynamics (MD) simulations. The most crucial aspect to build accurate MLPs is the *ab initio* (DFT) dataset used to train them, which should contain a large amount of diverse and independent atomic configuration (with the associated DFT energies and forces) to extensively cover the configuration space that will be explored during MD simulations.

The first stage of this study involved the construction of an initial dataset to train a preliminary version of the MLP, required as starting point in the active learning framework. To generate the atomic structures for the initial dataset, we performed MD simulations in LAMMPS [17] using the pretrained universal neural network potential CHGNet[18], producing long time-scales trajectories to be sampled and computed at the DFT level. In this phase, we considered the following systems: (i) ZDDP molecules and ZDDP isomers in a periodic box at temperatures ranging from 100 K to 5000 K, and (ii) ZDDP and ZDDP isomers molecules interacting with an Fe(110) slab at temperatures between 100 K and 1400 K. The use of elevated temperatures facilitated sampling of high-energy configurations, which are essential for constructing a robust training dataset that produces stable potentials even in harsh tribological conditions. Trajectories from these simulations were subsequently sampled to extract the most diverse and uncorrelated configurations, for which energies and forces were computed with DFT using the plane waves code of Quantum ESPRESSO (version 7.3)[19–21]. Specifically, we performed spin-polarized calculations with a kinetic energy cutoff for the wave functions of 60 Ry, and a cutoff for charge densities of 480 Ry. The exchange-correlation functional was described using the generalized gradient approximation (GGA) within the Perdew-Burke-Ernzerhof (PBE) parametrization[22]. We used PAW (Projector Augmented-Wave) pseudopotentials and included a gaussian smearing with a 0.00735 Ry width. Finally, dispersion interactions were included using the Grimme-D3 correction scheme[23].

The resulting initial dataset, comprising 710 frames, was later expanded by incorporating additional systems through our group's Strategic Configuration Sampling (SCS) active learning framework, whose workflow is accurately described in Ref. [13]. The software enables the simultaneous execution of the active learning procedure across multiple systems. This capability allowed us to incorporate a broad range of systems relevant to ZDDP tribofilm formation, including:

- diverse ZDDP molecules, such as linkage isomers (obtained through S-to-O exchange within the molecule [12]), oxidized derivatives (obtained through S-to-O substitution [12]), and molecules with different terminal groups (e.g., methyl, primary butyl, secondary butyl);

- various Fe-based substrates, including bulk phases, crystalline surfaces (e.g., (110), (210), (100)), defective surfaces with vacancies and steps, Fe surfaces partially passivated with oxygen (25% coverage), and also interacting with O_2 and H_2O molecules to explore spontaneous surface oxidation;

- bulk compounds representative of species commonly identified in ZDDP tribofilms, namely

ZnS, ZnO, $ZnFe_2(P_2O_7)_2$, $Zn_2P_2O_7$, $Zn_3(PO_4)_2$, $FePO_4$, and FeS_2. For these systems, a melt-quench protocol was applied during the exploration stage to generate amorphous bulk structures; then vacuum in the z direction was added to each generated bulk to sample also the corresponding surfaces;

- combined systems consisting of ZDDP molecules interacting with the aforementioned substrates under tribological conditions.

The active learning protocol was initially carried out using DeePMD MLPs, and MACE was used for the final iterations involving oxides, to produce a final dataset (16590 structures) that comprises all the aforementioned systems. Overall, three neural network potentials were employed for the molecular dynamics simulations: (i) a DeePMD-kit model (from now on referred to as DP), trained on an earlier version of the dataset that does not contain iron oxides, (ii) a MACE model (referred to as MACE), trained on a later version of the dataset that contains more structures for each system (and a few iron oxides-related structures), and (iii) a fine-tuned MACE model (referred to as MACE-FT), based on the pretrained universal potential MACE-MATPES-PBE-0 [24] [25] and trained by multi-head finetuning on the latest version of our dataset which includes a larger amount of iron oxides-related configurations. Each of these potentials were validated against the DFT reference data. In particular, we assessed their accuracy in two ways: with "physical" tests (dissociation energies, isomerization energies, and reaction barriers over a few notable reaction pathways), and "synthetic" tests, checking the agreement between predicted and reference DFT forces over the dataset through parity plots (both against their own training datasets, and the final dataset). All these tests can be found in the Supplementary Information (SI).

B. Molecular Dynamics Simulations

Once the reliability of our trained MLP was assessed, we performed different sets of molecular dynamics simulations. To do so, we used the LAMMPS [17] software, which supports the use of both MACE and DeePMD-kit potentials as force fields.

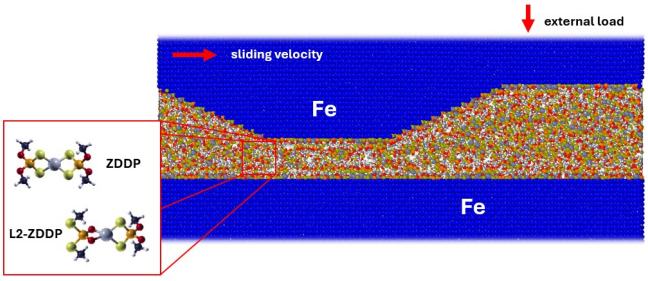

FIG. 1: One of the system used for molecular dynamics simulations.

The simulated systems, an example of which is depicted in Fig. 1, consisted of different size and orientation of Fe slabs intercalated with a molecular layer composed either of normal ZDDP molecules or LI2-ZDDP linkage isomers, obtained by double S-to-O exchange within the molecule[12]. The initial positions of the molecules within the interfacial region were obtained by random packing using the Packmol code [26].

In particular, four different surface geometries were considered:

- Fe(110): this is the most stable (lowest surface energy) Fe surface orientation. We used a cell size of 5.73 nm × 5.26 nm × 9.47 nm, containing 250 molecules within an interface of two specular Fe(110) slabs (1.15 nm thick), for a total of 14030 atoms.

- Fe(210): representative of a more reactive, rougher iron surface. We used a cell size of 5.76 nm × 5.15 nm × 9.50 nm, containing 250 molecules within an interface of two specular Fe(210) slabs (1.25 nm thick), for a total of 13230 atoms.

- FeO_x oxidized Fe(210) surface: a pseudo-amorphous oxide layer was included by spontaneous passivation from a mixture of O_2 and H_2O through molecular dynamics simulation (details are reported in the SI). We used a cell size of 11.50 nm × 5.15 nm × 12.50 nm, containing 500 ZDDP molecules within an interface of two specular oxidized Fe(210) slabs (∼1.50 nm thick, with a ∼0.7 nm surface oxide layer), for a total of 30885 atoms.

- large scale geometry with a Fe tip: this aims to simulate an asperity on the upper slab, with Fe(110) as the main surface and Fe(210) on the sides. The counter surface (lower slab) is Fe(110). The cell size is 20.93 nm × 4.87 nm × 25.56 nm, containing 700 molecules for a total of 99348 atoms.

In all the simulations, the bottommost Fe layer was fixed whereas the remaining atoms were divided into groups corresponding to lower/upper Fe slabs and confined molecules. Temperature control was applied separately to the Fe substrates and molecular layer using Nosé-Hoover thermostats. Two independent, same-T thermostat regions placed at the cell boundaries, spatially separated from the shearing interface, have been employed. Only these boundary "reservoirs" are thermostatted; the interfacial slab evolves according to the standard Newton's equations of motion with imposed external load and constrained constant relative velocity for the outmost iron layers.

For the flat Fe(110) and Fe(210) surfaces the MACE potential was used, while we employed the MACE-FT model and the DP model for the oxidized Fe(210) and the large scale tip geometry, respectively.

To obtain further insights into the characteristic of linkage isomers, we performed an *ab initio* molecular dy-

namics simulation of a 15Å × 15 Å × 18 Å box containing 2 LI2-ZDDP molecules at 450 K temperature for 3 ps. We used the same computational parameters of the DFT calculations for the dataset; the integration of the equation of motions was performed through the Verlet algorithm with a timestep of 1.45 fs, using the Bussi-Donadio-Parrinello (SVR) thermostat [27] to control the temperature.

Finally, Nudged Elastic Band (NEB) calculations [28] have been performed to evaluate the energy barriers across different transition states observed in the molecular dynamics simulations. We used the NEB module of Quantum Espresso, again with the aforementioned computational parameters, including 10 images (two fixed extrema and 8 optimizable), with a force threshold of 0.05 eV/Å on the elastic band and enabling climbing image.

III. RESULTS AND DISCUSSION

A. Testing of MLP's Accuracy

To assess the accuracy of the machine learning potentials (MLPs) developed in this work, we generated parity plots comparing atomic forces predicted by the models against ab initio reference data. The parity plots obtained for the MACE MLP are enclosed in the Supplementary Information, in Fig. S1. For most systems in the training dataset, the agreement between MLP forces prediction and DFT forces is excellent, as the majority of the force values cluster tightly around the diagonal, with only minor deviations at higher force magnitudes. Larger deviations are obtained for Fe surfaces, which contain defects and steps, either manually introduced or resulting from the high temperatures and pressures of the simulations from which they were sampled. In these non-equilibrium geometries, subtle changes in magnetic ordering or spin polarization can lead to significant variations in local forces, making them inherently more challenging both at the DFT level itself and in training the MLP. A more detailed discussion on this is included in the SI. However, even considering these larger discrepancies, the resulting root-mean-square error (RMSE) on the predicted forces falls well within the widely accepted range of 0.15-0.5 eV/Å for reliable interatomic potentials, confirming that the models capture the relevant physics with good fidelity[29, 30]. The active learning cycle allowed the dataset to progressively sample diverse atomic environments, spanning both equilibrium and non-equilibrium regions, which further enhanced the robustness of the trained potential. These results indicate that the SCS-generated potential can reproduce reference-level forces with sufficient accuracy to be used in large-scale molecular dynamics simulations beyond the reach of direct ab initio methods. An extended comparison on the accuracy of the three MLPs (DP, MACE, MACE-FT) employed in this work is reported in the SI, with comparison of predicted force errors on the DFT dataset (Fig. S2), and on a few notable reaction pathways by recomputing energies resulting from NEB calculations performed with DFT (Fig. S4 and Fig. S5). To further assess the reliability of our MLPs, we benchmarked dissociation and isomerization energies against reference *ab initio* data. Table I summarizes the calculated isomerization and dissociation energies obtained with density functional theory (DFT) and the three machine learning potentials. The configurations used for the three dissociative pathways correspond to those presented in our previous work Ref.[9]. For the isomerization energies, we considered the single and double S-to-O substitutions, corresponding to the LI1-ZDDP and LI2-ZDDP structures described in Ref.[12]. A summary of the considered configurations is also reported in the SI, Fig. S3. Differently from all the other MLP tests, in this case we relaxed the structures with each MLP instead of simply calculating the static energy.

	DFT	DP	MACE	MACE-FT
LI1-ZDDP	-0.15	0.28	-0.07	-0.13
LI2-ZDDP	-0.16	1.05	0.06	-0.06
Dissociation 1	-5.40	-6.03	-5.11	-
Dissociation 2	-6.89	-7.14	-6.36	-6.64
Dissociation 3	-10.92	-11.59	-10.73	-10.72

TABLE I: Test of MLP models accuracy on isomerization energies for the two linkage isomers (LI1-ZDDP and LI2-ZDDP) with respect to the normal ZDDP molecule, and dissociation energies for three dissociative configurations of the normal ZDDP, represented in Fig. S3.

It is worth noting that the DFT energies reported here differ slightly from those shown in the reference, due to minor variations in the computational setup employed. The two isomerizations (LI1-ZDDP and LI2-ZDDP) exhibit small energy differences at the DFT level, with values of –0.15 and –0.16 eV, respectively. The DP model significantly overestimates the isomerization energies, predicting them to be thermodynamically less stable than regular ZDDP, particularly for LI2-ZDDP, whereas both MACE and MACE-FT yield results much closer to the DFT reference, with MACE-FT being the only one that correctly predicts both as more thermodynamically stable.

For the dissociation reactions, all machine learning models qualitatively capture the energetic trends predicted by DFT. The DP model tends to slightly overbind, leading to more exothermic dissociation energies (by roughly 0.3–0.6 eV), while MACE achieves better quantitative agreement across all cases. The fine-tuned MACE-FT model shows the best overall correspondence with DFT, particularly for Dissociation 2 and 3, where deviations are below 0.3 eV. For dissociation 1, the MACE-FT value is not reported, as a further dissociation occurred, making the direct comparison not applicable, but this is not regarded as an issue given the extremely low dissociation barriers that are involved in these processes.

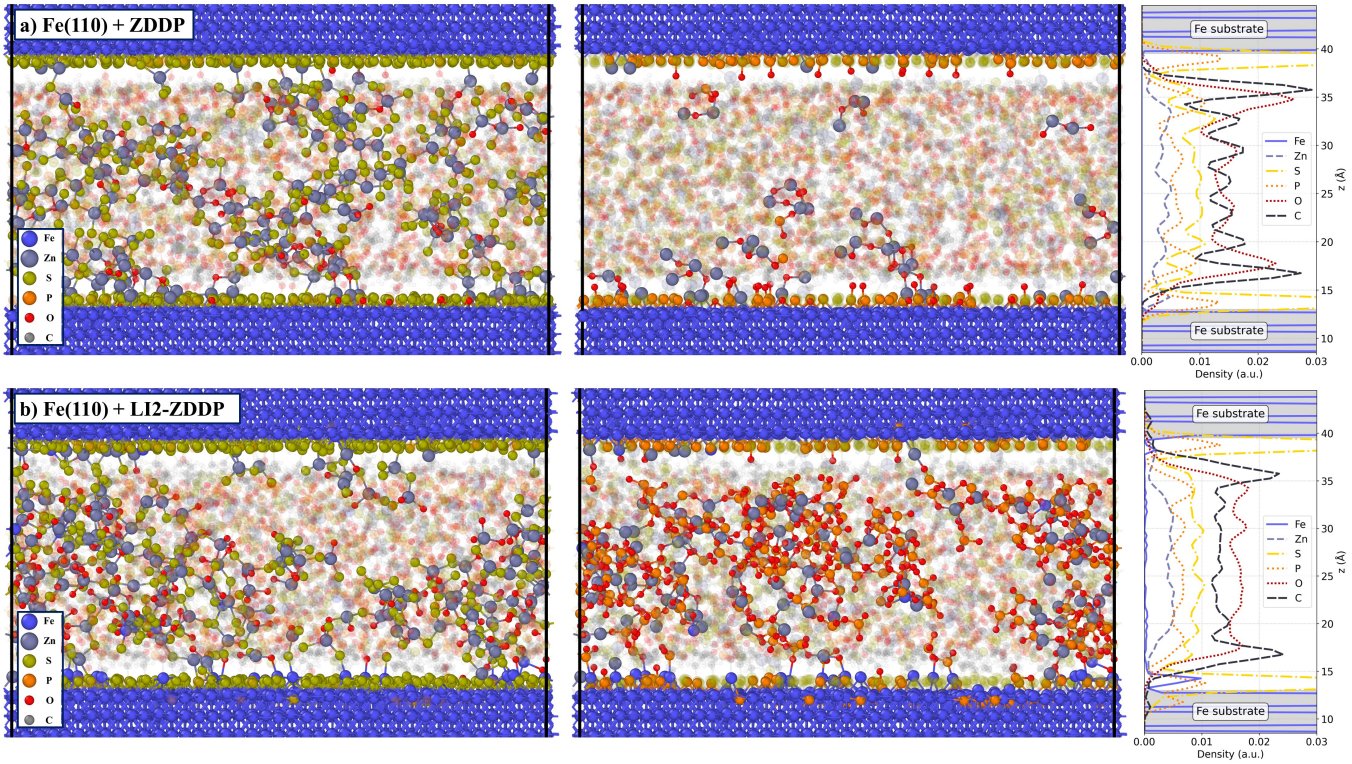

FIG. 2: Final snapshot of MD simulation of Fe(110)-Fe(110) interface with ZDDP (a) and LI2-ZDDP (b) at 2 GPa load and 450 K and 50 m/s sliding velocity after 30 ns, highlighting clusters containing Zn,S,Fe (left) and Zn,P,O,Fe (center), with planar-averaged atomic density (right).

B. Effect of Substrate Reactivity and Linkage Isomers on Tribofilm Formation

Zinc dialkyldithiophosphate (ZDDP) is known to form protective tribofilms on a wide range of surfaces, from ferrous substrates to ceramics. The strength and durability of these tribofilms, however, depend strongly on the underlying substrate. Furthermore, numerous phenomena influence the rate and stability of tribofilm growth, leading to a complex interplay of factors that are often challenging to disentangle experimentally. In this work, we investigate the influence of different substrates on ZDDP tribofilm formation.

We first examined the most energetically stable Fe surface, namely Fe(110). To assess the effect of enhanced surface reactivity, we then simulated Fe(210) surfaces. These simulations were performed using the MACE model. Next, to explore geometric effects, we simulated a large-scale Fe interface featuring an asperity. Due to the size of this system, nearly 100,000 atoms, we employed the DP model, which provides lower computational costs while maintaining reasonable accuracy. Finally, to evaluate the impact of surface chemistry, we included oxidized Fe surfaces. As simulations of Fe oxides are particularly challenging, we used the MACE-FT model, which was fine-tuned on our dataset starting from a pretrained universal potential. Although the fine-tuned model has a higher computational cost compared to the MACE model trained from scratch (due to the larger cutoff radius of the pretrained potential), we used it to ensure higher fidelity.

	P-O-P	O-Fe-O	Zn-O-Zn	**Zn-S-Zn**
Fe(110)-N	0	6	89	191
Fe(110)-LI2	82	11	19	184
Fe(210)-N	0	3	43	297
Fe(210)-LI2	76	79	20	179
Fe tip-N	1	42	6	624
Fe tip-LI2	262	111	26	385
FeO_x-N	22	-	21	153
FeO_x-LI2	65	-	37	146

TABLE II: Number of A-B-C bonds at the end of the MD simulation for the different surface-molecule combination. Normal (N) ZDDP does not form polyphosphate networks (P-O-P) on non-oxidized Fe, while LI2-ZDDP forms large Zn/Fe polyphosphate clusters with O atoms bridging Fe/Zn cations to the phosphate network. For the oxidized surface, a small amount of polyphosphates in observed also for normal ZDDP. Both normal and LI2 ZDDP form ZnS, in larger amount for normal ZDDP compared to LI2. The horizontal lines separate the different groups of simulations that are not directly comparable in absolute values due to the different system sizes and number of molecules. For oxidized surfaces, the O-Fe-O bond count was not reported as not meaningful since those bonds are also present in the oxide layers.

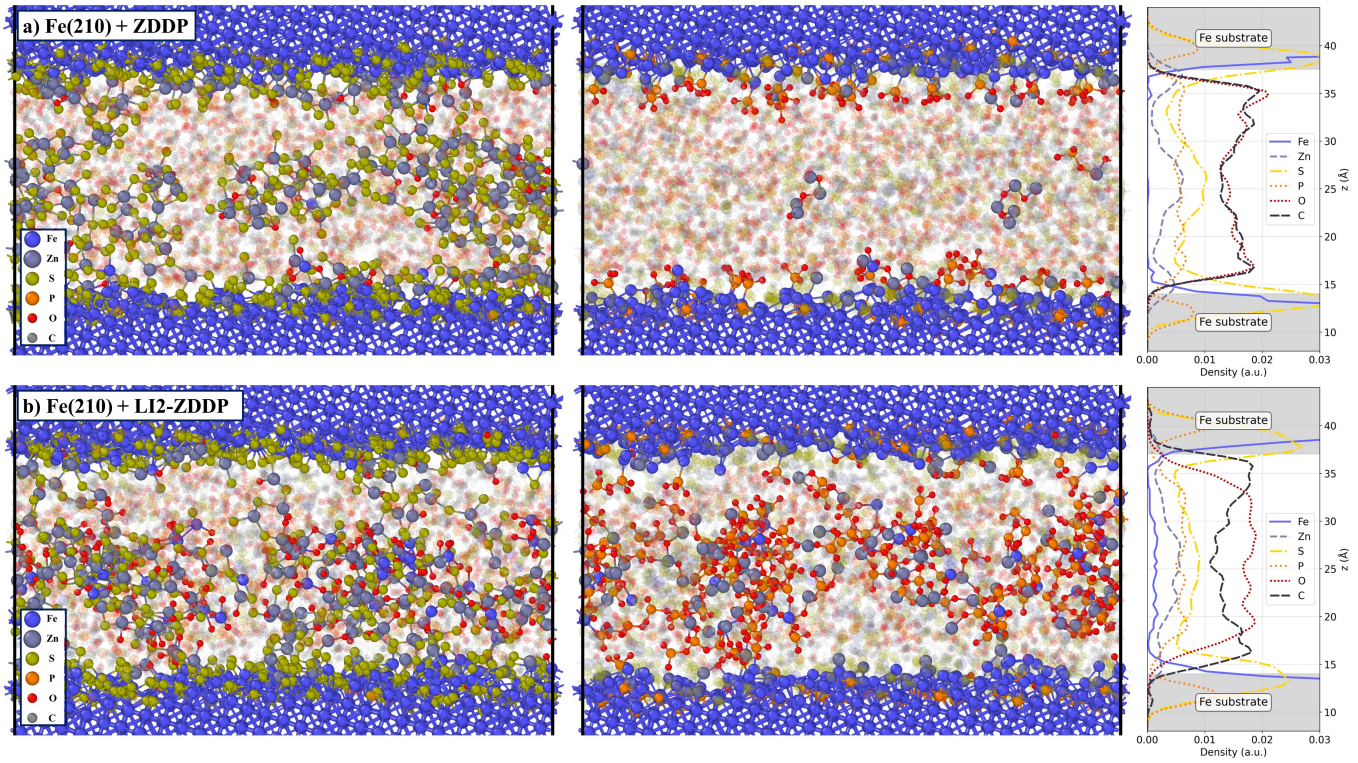

FIG. 3: Final snapshot of MD simulation of Fe(210)-Fe(210) interface with ZDDP (a) and LI2-ZDDP (b) at 2 GPa load, 450 K and 50 m/s sliding velocity after 30 ns, highlighting clusters containing Zn,S,Fe (left) and Zn,P,O,Fe (center), with planar-averaged atomic density (right).

For the smaller systems (flat iron surfaces and oxidized surface) we applied a normal load of 2 GPa and maintained a temperature of 450 K. A sliding velocity of 50 m/s and 10 m/s was used for the flat iron surfaces and the oxidized surface, respectively. The large-scale asperity systems were simulated under a 1 GPa normal load on the external layer (which results in a higher load on the region under the asperity), at 350 K, and with a sliding velocity of 5 m/s.

Since molecular isomerization has been reported as a key step in ZDDP dissociation pathways, we also investigated how starting from already formed LI2-ZDDP isomers influences the associated tribochemical reactions.

For the less reactive Fe(110) interface, simulations revealed that both ZDDP (Fig. 2a) and LI2-ZDDP (Fig. 2b) molecules rapidly adsorb onto the substrate, leading to a full passivation of the Fe surface mainly by S and P atoms (and on smaller amount by Zn atoms), as shown by the atomic density profiles along the z-axis (right panels), which exhibit sharp S and P peaks. Consequently, the surfaces quickly become inert. As sliding continues, however, differences between the two isomers emerge. In the central region of the interface that contains the molecular fluid, we observe the formation of Zn–S clusters for both ZDDP and LI2-ZDDP, though they are less prominent for the latter, as indicated by the Zn-S-Zn bonds count in Tab. II. Interestingly, a (Zn) polyphosphate network appears exclusively in the LI2-ZDDP case, as visible in the figures and from the P-O-P bonds count in Tab. II, suggesting that isomerization plays a crucial role in the formation of the polyphosphate networks experimentally observed in ZDDP tribofilms. A small amount of Fe is released from the surface into the interfacial region (few atoms), which is compatible with experimental findings where Fe is typically incorporated within ZDDP tribofilms formed on Fe substrates, although involving a much smaller quantity due to the low surface reactivity combined with the short time scales of the simulations compared to experiments. In both systems, the Fe surfaces remain mostly structurally stable. In contrast to normal ZDDP, however, for LI2-ZDDP a few Fe atoms are displaced from the surface (replaced by P, S or C) and partly integrated in the polyphosphate network, as shown by the atomic density profiles, indicating a higher reactivity for the isomer.

On the Fe(210) surfaces, the enhanced surface reactivity results in the development of an amorphous FeS layer containing interspersed P and Zn atoms, as revealed by the atomic density profiles. Within the lubricant film, ZnS clusters form for both ZDDP, in Fig. 3a and LI2-ZDDP, in Fig. 3b. Even on such short timescales compared to experimental times, the amorphous FeS surface layers are already slowly growing by incorporating S and Zn from the fluid domain, leading to the formation of the FeS/ZnS region that is experimentally observed as

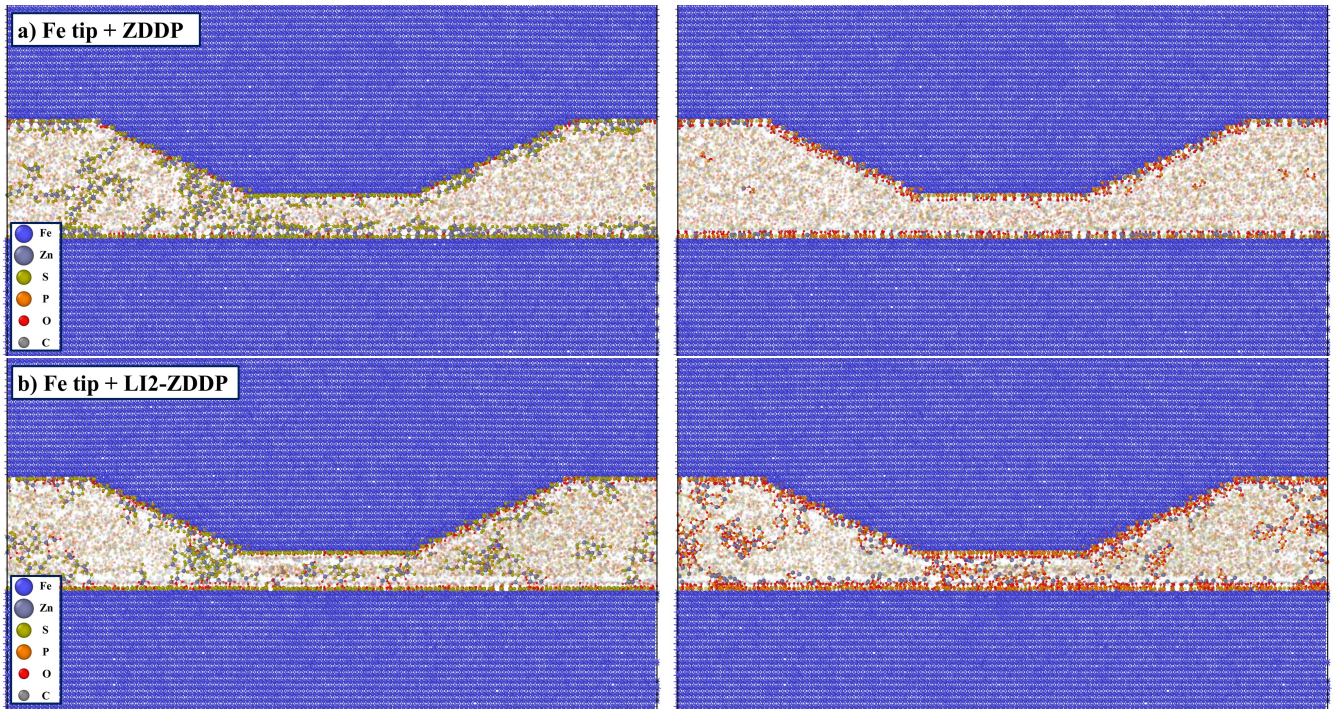

FIG. 4: Final snapshot of MD simulation of Fe-Fe interface including an asperity with ZDDP (a) and LI2-ZDDP (b) at 1 GPa load and 350 K and 5 m/s sliding velocity after 23 ns, highlighting clusters containing Zn,S,Fe (left) and Zn,P,O,Fe (center), with planar-averaged atomic density (right).

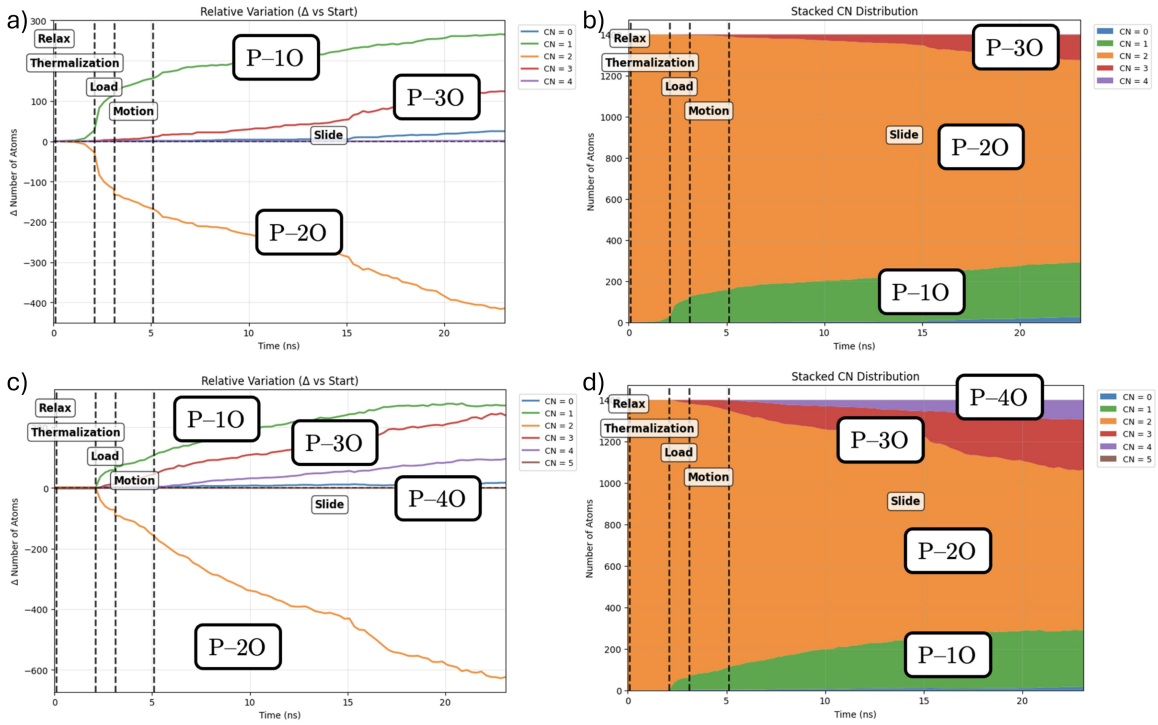

FIG. 5: P–O relative (a,c) and stacked (b,d) coordination number analyses performed on the molecular dynamics trajectories for ZDDP (upper panel) and LI2-ZDDP (lower panel). The P-nO labels indicate the number of O atoms bonded to each P atom. The smaller labels mark the simulation phases: first an initial geometry optimization (relax), then a thermalization with fixed boundaries and then a load ramp, finally a velocity ramp (motion) to reach the steady state sliding condition.

the tribofilm first layer in direct contact with the substrate [1]. Consistent with the behavior on Fe(110), Zn

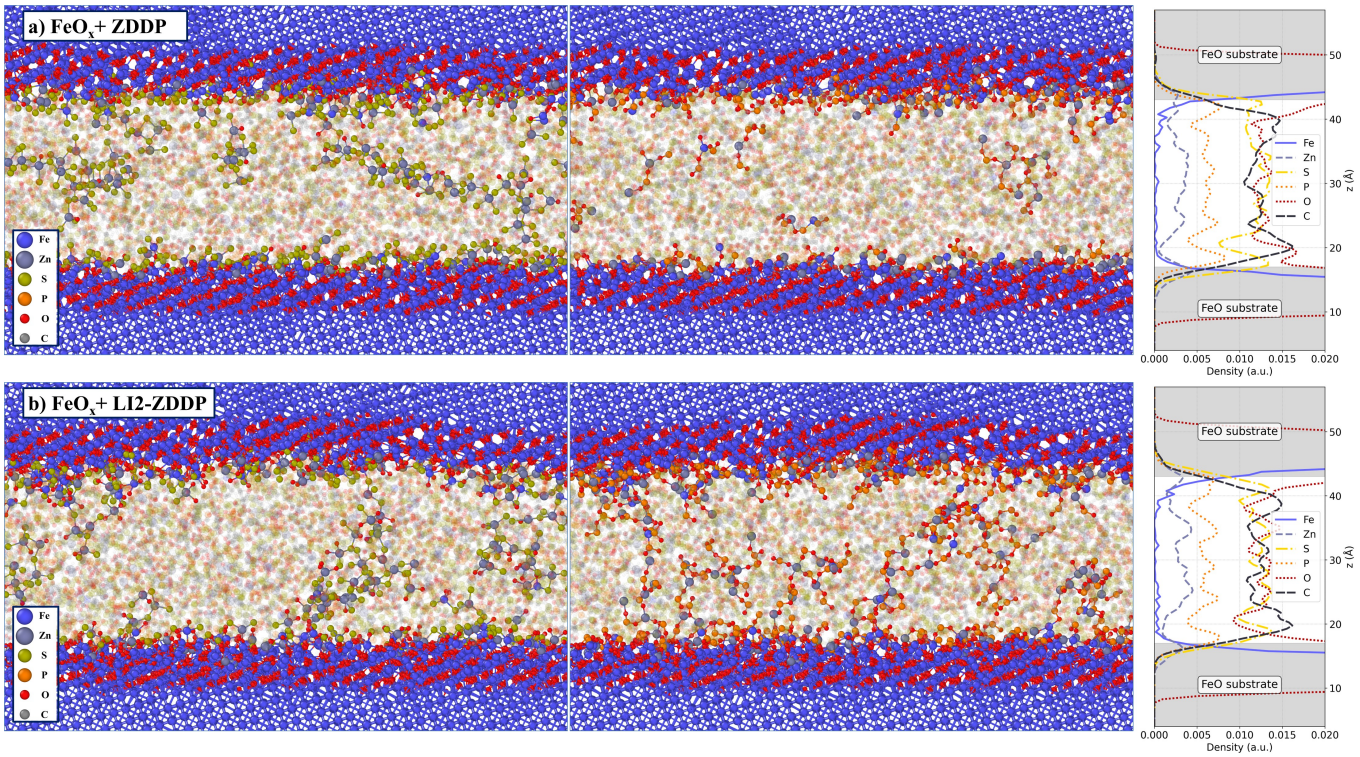

FIG. 6: Final snapshot of MD simulation of oxidized Fe interface with ZDDP (a) and LI2-ZDDP (b) at 2 GPa load, 450 K and 10 m/s sliding velocity after 10 ns, highlighting clusters containing Zn,S,O,Fe (left) and Zn,P,O,Fe (center), with planar-averaged atomic density (right).

polyphosphate networks appear only for LI2-ZDDP; however, in this case, a significantly larger fraction of Fe becomes incorporated into the phosphate network, as highlighted by the density profiles and by the O-Fe-O bonds count in Tab. II. This process is particularly interesting, as the progressive incorporation of Zn and Fe cations within the polyphosphate network is believed to be the main mechanism that leads to the hardening and increased wear-resistance of the tribofilm [1].

Then we considered a more realistic surface geometry, including an asperity. The system consists of a Fe interface composed of two Fe(110 slabs), the upper one containing an asperity (with Fe(210) on the sides). The general behaviour confirmed what we observed with systems of smaller scales, both upon visual inspection and from the bonds counts in Tab. II. During the simulations, the dissociation of the molecules was initiated by the rupture of Zn–S bonds, promoted by the strong interaction of sulfur and zinc atoms with the iron substrate, in agreement with previous theoretical predictions. This process resulted in the chemisorption of Zn and S species onto the metallic surface and marked the onset of tribofilm formation. A fraction of zinc atoms, initially chemisorbed, were partially released during the simulations, compatible with the loss of Zn from the surface observed in multiple experimental works [1]. Alkoxy groups in both systems remained chemically stable, while partial cleavage of C–S bonds occurred only in LI2-ZDDP.

The evolution of the P–O coordination, which is connected to the formation of polyphosphates, was monitored with the analysis of pairwise coordination number (Fig. 5). In particular, the values shown for each coordination number are normalized with respect to their initial values, and therefore indicate the variation in the number of species with that coordination state over the course of the simulation. The stacked coordination number distribution provides a complementary view based on absolute values. At each time frame, the number of atoms with a given CN is represented as a band in a stacked area chart, where the vertical thickness of the band corresponds to the absolute count. When read from left to right, the plot shows how the distribution of coordination numbers evolves throughout the trajectories. At a given time, the composition of coordination environments can be understood from the cumulative stacking of the bands. The P–O coordination evolution highlights the progressive development of phosphate networks, the structural foundation of the tribofilm. LI2-ZDDP displays a faster transition toward higher P–O coordination, forming also phosphate groups with four oxygen atoms, indicating accelerated polymerization and the formation of extended polyphosphate networks. Indeed, also in this case Zn polyphosphates (with a small incorporation of Fe) are found only in the system containing LI2-ZDDP. Notably, in both cases it's clearly visible that the application of load marks the start of chemical reactions involving P-O

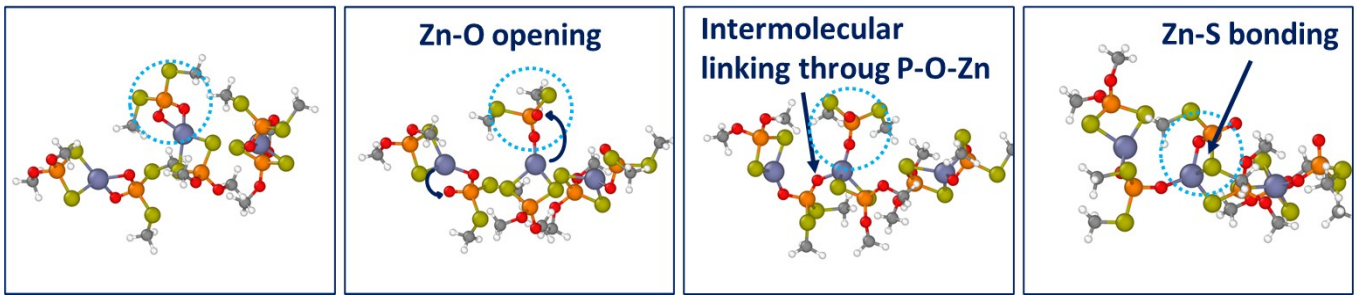

FIG. 7: Snapshots from the MD simulations of Fe(210) with LI2-ZDDP, following the evolution of three molecules. At the beginning of the simulation (left panel) the three molecules are close to each other in their original bonding configuration. Next, thermal motion opens the Zn-O bond of two molecules, forming reactive P=O structures with the exposed oxygen atoms. Then, A Zn-O bond is formed between the Zn of a molecule and the exposed O of the other molecule, which can be seen as the starting point for the formation of a Zn polyphosphate network. Finally, after a rotation of the opened phosphate group of the central molecule, the S-CH_3 group bonds to the central Zn, forming a structure akin to LI1-ZDDP in terms of coordination environment of the central Zn, but with the -R group bonded to S as in the initial LI2.

bonds, forcing molecules close to each other and therefore promoting bond formation. All these findings align with those emerged from the previous simulations. It's worth noticing the differences in the first tribofilm surface layer observed in the flat geometries for the Fe(110) and Fe(210) surfaces are reproduced also in the asperity. The Fe(110) regions are completely passivated (and saturated) by a monolayer of S and P atoms, with no subsurface diffusion, while the Fe(210) sides of the asperity exhibit a more amorphous surface film, also incorporating small amounts of Zn, with traces of S and P atoms intercalated in the subsurface Fe layers.

Finally, we considered an oxidized surface, obtained through a molecular dynamics simulation by spontaneous reactions between Fe(210) surfaces and a mixture of oxygen and water molecules. More details on this process are reported in the SI. As visible in Fig. 6, the presence of the oxide layer reduces the initial dissociation of both ZDDP and LI2-ZDDP molecules in contact with the surface, and the release of sulfur is slower. The adsorbed surface layer is also different, with fewer chemisorbed S and P, and a larger amount of Zn, mainly bonded to oxygen atoms of the surface oxide. This lower reactivity of oxidized surfaces towards the dissociation of ZDDP molecules compared to perfectly clean Fe surfaces confirms the observations in our previous work [9]. However, this does not mean that reactivity is suppressed, as will be explained in the following sections. Regarding the comparison between normal and LI2-ZDDP, the trends are similar to the previous cases, with LI2-ZDDP enabling the rapid formation of Fe/Zn polyphosphate clusters (the lower amount in the image compared to the Fe(210) simulations can also be attributed to the shorter simulation time – 10 ns vs 30 ns – and lower sliding speed – 10 m/s vs 50 m/s). However, in contrast with the non-oxidized Fe surfaces, the formation of a few initial polyphosphate structures is observed also for normal ZDDP, as visible from the images and in P-O-P bons count in Tab. II. This process seems to be enabled by the more reactive environment, that facilitates the alkyl groups cleavage from C-O bonds, allowing oxygen atoms in ZDDP to form P-O-P bonds. This aspect will be clarified in the next sections.

Collectively, our analyses across different substrates reveal that LI2-ZDDP undergoes more efficient dissociation, greater atomic mobility, and enhanced phosphate network formation, mechanistic features that explain its superior tribofilm-forming capability compared with the parent ZDDP. The presence of surface oxides appears to facilitate the reaction kinetics and the growth of phosphate chains, even (albeit at a slower rate) for normal ZDDP. However, oxidation is not a prerequisite for polyphosphate formation. Instead, the oxide layer modulates rather than determines the reactivity of the interface. This observation supports the view that the substrate plays an important, yet non-exclusive, role in the tribochemical process – consistent with experimental reports showing ZDDP-derived films forming on a variety of surfaces, including metallic iron, oxidized iron, and even DLC coatings.

C. Insights on the role of the LI2-ZDDP isomer in the formation of polyphosphates

All simulations presented in the previous section indicate that, regardless of substrate reactivity, LI2-ZDDP drastically accelerates the formation of the polyphosphate network that constitutes the tribofilm. We therefore examined in detail the role played by LI2-ZDDP in enabling polyphosphates formation.

In all simulations involving LI2-ZDDP, thermal motion induces the opening of some Zn-O bonds, causing the phosphate groups to re-arrange by exposing a P=O bond, as visible in Fig. 7. This is crucial as the exposed oxygen can naturally enable the formation of polyphosphates by bonding to nearby P atoms. This mechanism observed in our large scale molecular dynamics simulations with MLPs reproduces the findings of Mosey et al. with *ab initio* static calculations and molecular dynamics simulations [6, 11]

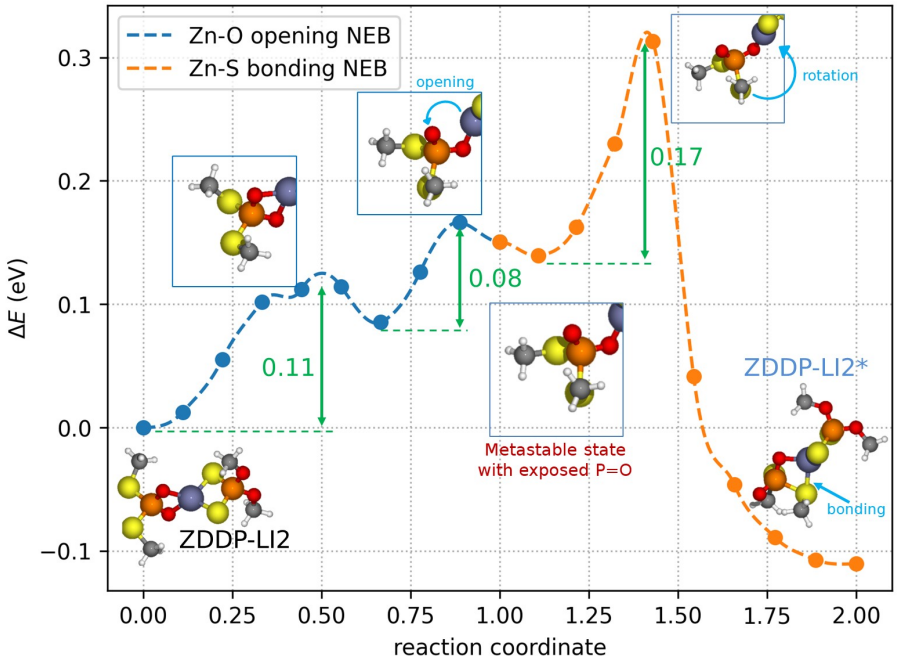

FIG. 8: *Ab initio* reaction pathway for the LI2-ZDDP self-isomerization to form a new isomer. It starts with the breaking of the Zn-O bond, forming a metastable phosphate group with a P=O double bond, and finally the rotation of the S-R group to bond to the central Zn, leaving now the oxygen exposed to bond with nearby phosphate groups to form polyphosphates.

Moreover, this Zn-O bond opening can then allow for further processes to occur, such intermolecular linking by forming a bond between the O of P=O and the Zn of another molecule, as visible again in Fig. 7, and the open phosphate group can rotate in such a way to form a bond between the external S-R group and the central Zn, forming a new isomer, which we called LI2*, similar to the LI1 isomer in terms of coordination environment of the central Zn, but with the -R group bonded to S as in the initial LI2.

To gain more insights into this Zn-O bond opening, rotation and formation of Zn-(S-R) bond, and to validate the MLP accuracy in the simulation of the reaction pathway, we carried out an *ab initio* MD simulation of two LI2-ZDDP molecules at 450 K. After some oscillations, the Zn-O bond of one molecule was stably opened after just 1 ps. In 2 ps, we also observed the rotation and formation of Zn-S bond, suggesting that the process has an extremely low reaction barrier. This was confirmed by carrying out a nudged elastic band (NEB) calculation between the initial and final states extracted from the *ab initio* MD simulation. As visible in Fig. 8, the whole process shows a few intermediate barriers, ranging from 0.11 eV to 0.17 eV, with lower barrier for the Zn-O opening to reach the metastable state with exposed P=O (which does in fact occur much more frequently in the large scale simulations) and a slightly higher barrier for the rotation and Zn-S bonding, reaching the LI2* configuration that is slightly more thermodynamically stable than the starting LI2-ZDDP (and hence more stable than the normal ZDDP). The MLPs (especially the MACE and MACE-FT models accurately reproduce this reaction pathway, as reported in Fig. S4.

Summarizing, these results seem to indicate that the increased reactivity of LI2-ZDDP isomer is directly related to the Zn-O bond opening, which enables both the formation of P-O-P bond when getting in close contact with another non-saturated P atom, and also intramolecular linking by forming P-O-Zn bonds. Moreover, the direct involvement of Zn atoms in the early stage of polyphosphate formation can accelerate the transition to a Zn polyphosphate structure, which is related to more resistant tribofilms.

D. Insights on alkyl chains removal

One of the open questions related to the formation of the tribofilm, which is experimentally found to be carbon-free, is how the terminal -R chains are removed during the tribochemical process. This is also strictly related to the formation of polyphosphates, as terminal -R units need to be removed to effectively form a polyphosphate network.

To shed some light on the evolution of hydrocarbons, we counted at different times during the simulations the number of C-O and C-S bonds, of C-$H_{(1,2,3)}$ units, of C participating in at least one C-C bond, and finally the number of -OH groups. We report the values in Tab. III for all the simulations involving flat surfaces - namely Fe(110), Fe(210) and oxidized Fe(210).

For normal ZDDP in the non-oxidized surfaces, neg-

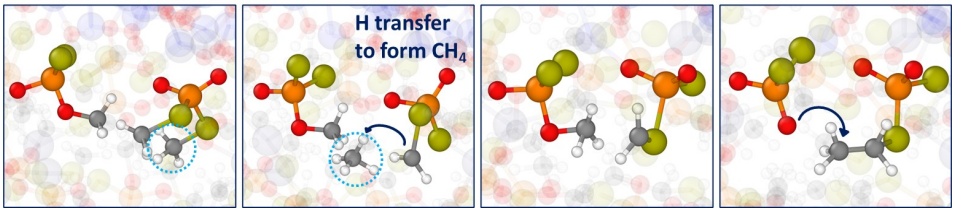

FIG. 9: Some reaction pathways that lead to the formation of hydrocarbon chains, the first step of removal that ultimately can lead to a carbon-free tribofilm. They highlight a wide variety of chemical pathways, possibly assisted by the presence of oxygen from oxide, which can act as a H acceptor.

		C-O	C-S	-CH	-CH_2	-CH_3	-C-	-OH
Fe(110)-N	t=0	1000	0	0	0	1000	0	0
	t=10 ns	999	1	0	0	1000	0	0
	t=30 ns	998	2	0	0	1000	0	0
Fe(210)-N	t=0	1000	0	0	0	1000	0	0
	t=10 ns	999	1	0	0	1000	0	0
	t=30 ns	996	3	0	0	1000	0	0
Fe(110)-LI2	t=0	500	500	0	0	1000	0	0
	t=10 ns	500	478	10	1	986	4	0
	t=30 ns	499	458	9	0	980	6	0
Fe(210)-LI2	t=0	500	500	0	0	1000	0	0
	t=10 ns	500	443	0	0	990	2	0
	t=30 ns	498	419	1	1	987	6	0
FeO_x-N	t=0	2000	0	0	0	2000	0	390
	t=10 ns	1513	413	96	312	1431	177	838
FeO_x-LI2	t=0	1000	1000	0	0	2000	0	390
	t=10 ns	804	1091	71	335	1485	135	750

TABLE III: Number of C-O and C-S bonds, of -CH, -CH2 and -CH3 groups, number of C atoms participating in hydrocarbon chains (bonded to at least another C), and of -OH groups for flat surfaces simulation, at the beginning of the (t=0), after 10 ns, and after 30 ns (only for the non-oxidized surfaces). Normal ZDDP is denoted by *N*.

ligible C-O bond cleavage occurs, resulting in a transfer from O to S, but no formation of chains, and no hydrogen transfer. Since all -R groups are bonded to O, this means that no oxygen atoms are free to participate in the formation of polyphosphate networks, explaining the observations from the MD simulations and the absence of P-O-P bonds.

For LI2-ZDDP the picture is completely different: half of -R groups are bonded to S, and the C-S bond appears to be easier to break (roughly 8% decrease for Fe(110) and 16% for Fe(210) in 30 ns), in agreement with our previous *ab initio* calculations [12]. At the same time, a few small chains are formed, with 6 C atoms bonded to other C atoms at the end of both simulations. Some CH and CH_2 also appear, indicating more overall reactivity of the LI2 isomer compared to normal ZDDP. A negligible decrease in C-O bonds is observed also for LI2; however, as explained more in detail in the previous section, this does not prevent the formation of polyphosphate networks, as half of the oxygen atoms in the molecule are not bonded to C and are therefore free to participate in reactions.

The oxidized surface, instead, exhibits a markedly different behaviour. Here, a large number of C-O bonds are broken, both for normal and LI2 ZDDP, with a decrease of 20% and 24%, respectively. This seems to follow from the initial attack by oxygen atoms of the surface oxide layer and small iron oxides cluster that disperse into the liquid. These processes cause H transfer from -CH_3 groups to form -OH terminations, as observed by the massive decrease in -CH_3 to form -CH_2 and -CH units, and the concurrent increase in -OH groups (the initial number is from terminal -OH and adsorbed water molecules initially present on the oxidized surface). The process eventually leads to the formation of hydrocarbon chains, with more than 100 C atoms forming at least one C-C bond for both normal and LI2 ZDDP. These C-O bond breaking events explains why some P-O-P bonds were formed also for normal ZDDP, albeit in a significantly lower amount than for the LI2 isomer, as the latter has also two oxygens that are non bonded to carbon, as discussed above.

We looked closely into some atomistic processes involving the reaction of hydrocarbon chains from the MD simulation of LI2-ZDDP with the oxidized surface. Fig. 9 shows a process which starts with an intra-molecular transfer of H from one of the two S-CH_3 to the other, releasing CH_4, and finally leading to an intermolecular O-CH_3 transfer, cleaving the C-O bond to form a S-CH_2-CH_3 chain. Analogous processes were also observed in the non-oxidized simulations, as they do not involve iron or oxygen, and they account for the small amount of C-O decrease and formation of C-C bonds.

Another, more complex reaction is reported in Fig. 10. It starts with an H transfer from -CH_3 to an O of a P=O bond from an "opened" phosphate group of another LI2-ZDDP. The remaining O-CH_2 bonds to an S a further H transfer to S to form a thiol takes place. From a nearby molecule, a collective process involving H_2 emission and H-to-S transfer leads to the formation of a first C-C bond, creating a S-C-CH_2 termination. This reactive complex then form a second bond to the initially formed CH_2, and an internal H transfer leads a cyclopropane-like unstable intermediate, which rapidly transforms into a more stable, 4-carbons chain where all C atoms are either in sp^2 or sp^3a arrangement. In the meantime, the previously dissociated H_2 diffuses through the solution, forming a methane with another -CH_2 group.

A third notable reaction, which is started by the pres-

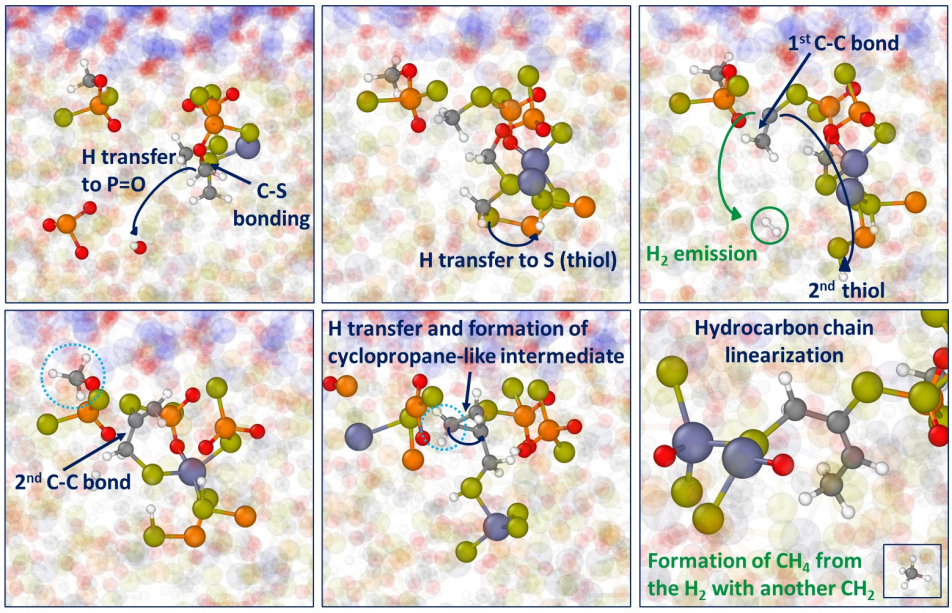

FIG. 10: Some reaction pathways that lead to the formation of hydrocarbon chains, the first step of removal that ultimately can lead to a carbon-free tribofilm. They highlight a wide variety of chemical pathways, possibly assisted by the presence of oxygen from oxide, which can act as a H acceptor.

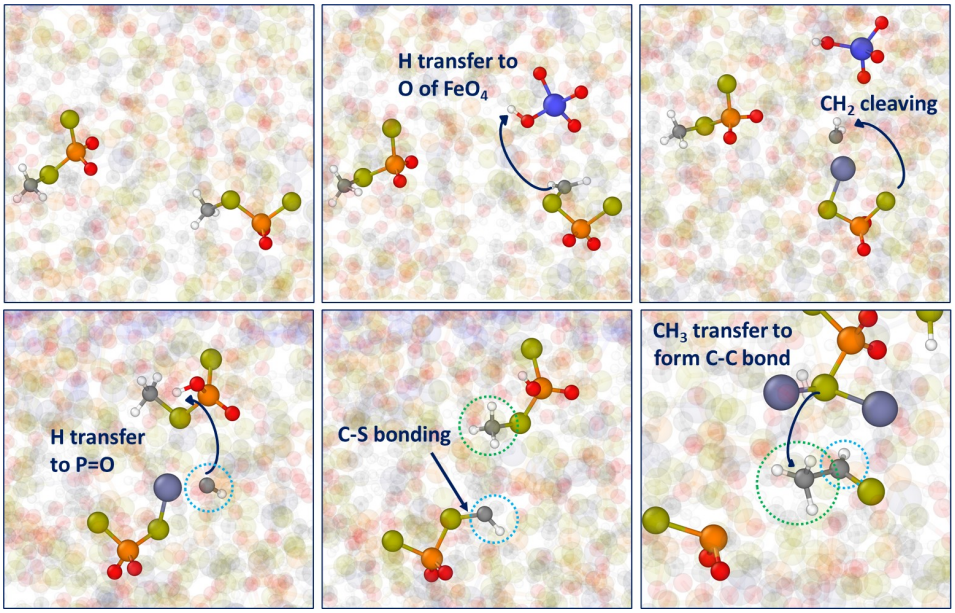

FIG. 11: Some reaction pathways that lead to the formation of hydrocarbon chains, the first step of removal that ultimately can lead to a carbon-free tribofilm. They highlight a wide variety of chemical pathways, possibly assisted by the presence of oxygen from oxide, which can act as a H acceptor.

ence of iron oxide, is depicted in Fig. 11. First, an H atom is transferred from a CH_3 to an O of a FeO_4 cluster, forming an -OH group. Then, CH_2 cleaving due to thermal motion and a further H transfer to a P=O eventually lead to the formation of a S-C-CH_2 termination. From the amount of -OH groups formation that appears from the bond analysis discussed above, the process involving an intial H transfer, leading to reactive pathways that follow from the creation of unstable -CH_2 termination seem to play a key role in the significantly larger reactivity exhibited even by normal ZDDP in the oxidized environment.

The growth of hydrocarbon chains that we observed is the initial step that can produce fully-saturated chains, which, no longer bonded to the reactive atoms of ZDDP, can be removed by clustering with oil in the solution.

To ensure the realism of the processes observed in the simulation, the energy barriers of a few of the aforemen-

tioned reactions were individually calculated by means of *ab initio* NEB calculations and re-calculated on the static images by the three MLPs. The results are reported in Fig. S5.

E. Summary of tribofilm formation mechanisms

The overall picture that emerges from the comparative analysis and the investigation of atomistic reaction processes is the following:

- More reactive, atomically-rougher Fe surfaces, such as the Fe(210), enhance the growth of the first FeS/ZnS layer, and also the release of Fe atoms to participate in the hardening of the tribofilm by incorporation into the polyphosphate network
- The formation of polyphosphate networks is subject to the availability of "exposed" O atoms that can participate in either P-O-P, P-O-Zn or P-O-Fe bonding
- The LI2 isomer naturally provides exposed O atoms by the opening of Zn-O bonds with the central Zn atom, resulting in a metastable structure with P=O bonds. This behaviour was thoroughly demonstrated in this study both by *ab initio* and machine learning MD simulations, by computing reaction barriers, and is in agreement with previous *ab initio* studies. In case of low-reactivity environment, the ability of ZDDP to self-isomerize may be the key step that drives polyphosphate formation
- In more reactive environments, such as oxidized surfaces, the generation of exposed O atoms is partially provided by complex reaction pathways that revolve around H transfer and result in enhanced C-O bond cleavage even for normal ZDDP. We hypothesize that similar reaction pathways could however be enabled also by the presence of molecular O_2 or other radicals present in the solution, in absence of an oxidized surface. For such reactive environments, the role of isomerization seems to be smaller, and polyphosphate formation can be achieved directly from normal ZDDP (albeit at a lower rate).

IV. CONCLUSIONS

In this work, the atomistic mechanisms that lead to the formation of anti-wear tribofilm from ZDDP lubricant additives are unraveled through machine learning-based molecular dynamics (ML-MD). Accurate machine learning potentials (MLPs) are trained by means of an active learning approach, and the atomic trajectories are analyzed both qualitatively and quantitatively through the calculation of coordination numbers (CN), bonds counting, cluster analysis and NEB calculations. The simulations reveal that the initial dissociative chemisorption occurs immediately under applied load, while the subsequent growth of the film and formation of polyphosphates are primarily activated by sliding. Sliding drives continuous bond breaking and formation, initiating the development of an iron sulfide layer and polyphosphate networks that represent the early stages of the amorphous nanocrystalline anti-wear film. The LI2-ZDDP isomers,obtained through double S-to-O exchange in the standard ZDDP molecule, are more reactive than ZDDP, promoting faster polyphosphate formation. While ZDDP retains intact alkoxy groups, LI2-ZDDP shows alkyl detachment and chemisorption onto the Fe substrate. Metal atoms, including Fe from the substrate and Zn from dissociated ZDDP (some of which desorb from the surface after initial chemisorption), integrate into the evolving phosphate network, forming mixed polyphosphates. Overall, the early stages of tribofilm formation involve a dynamic interplay of adsorption, bond breaking, rehybridization and intermixing of Fe atoms into the polyphosphate structures, highlighting the complexity of the mechanochemical processes that initiate the tribofilm development. These findings provide fundamental understanding of the atomic-scale mechanisms that govern ZDDP's performance as anti-wear additive and predicts that isomerization is a key step for the formation of phosphate networks. In conclusion, the results of this study indicate that ZDDP exhibits such high reactivity and such a wide range of dissociation pathways that it is ultimately able to form a tribofilm under a variety of conditions and on different substrates. The multiplicity of possible mechanisms makes the film formation process highly dependent on the experimental setup, which determines the dominant pathway. This intrinsic complexity may explain why, despite decades of research, a unified and universally accepted description of the sequence of mechanisms leading to tribofilm formation has yet to emerge.

ACKNOWLEDGEMENT

These results are part of the SLIDE project, which received funding from the European Research Council (ERC) under the European Union's Horizon 2020 research and innovation program. (Grant Agreement No. 865633).
M.C. Righi acknowledges the European Union - NextGeneration EU (National Sustainable Mobility Center CN00000023, Italian Ministry of University and Research Decree n. 1033 - 17/06/2022, Spoke 11 - Innovative Materials & Lightweighting). The opinions expressed are those of the authors only and should not be considered as representative of the European Union or the European Commission's official position. Neither the European Union nor the European Commission can be

held responsible for them.
M.C. Righi acknowledges support by ICSC - Centro Nazionale di Ricerca in High Performance Computing, Big Data and Quantum Computing, funded by European Union - NextGeneration EU.
We acknowledge the CINECA award under the ISCRA initiative, for the availability of high-performance computing resources and support.

[1] H. Spikes, Mechanisms of zddp—an update, Tribology Letters **73**, 38 (2025).
[2] S. Korcek and M. Nakada, Engine oil performance requirements and reformulation for future gasoline engines and systems, SAE transactions , 909 (1996).
[3] D. Uy and A. E. O'Neill, Raman studies of automotive catalyst deactivation, SAE Transactions , 136 (2006).
[4] P. Parsaeian, A. Ghanbarzadeh, M. C. Van Eijk, I. Nedelcu, A. Neville, and A. Morina, A new insight into the interfacial mechanisms of the tribofilm formed by zinc dialkyl dithiophosphate, Applied Surface Science **403**, 472 (2017).
[5] R. Heuberger, A. Rossi, and N. D. Spencer, XPS study of the influence of temperature on ZnDTP tribofilm composition, Tribology Letters **25**, 185 (2007).
[6] N. J. Mosey and T. K. Woo, A quantum chemical study of the unimolecular decomposition mechanisms of zinc dialkyldithiophosphate antiwear additives, The Journal of Physical Chemistry A **108**, 6001 (2004).
[7] N. J. Mosey, M. H. Muser, and T. K. Woo, Molecular mechanisms for the functionality of lubricant additives, Science **307**, 1612 (2005).
[8] S. Peeters, A. Barlini, J. Jain, N. N. Gosvami, and M. Righi, Adsorption and decomposition of zddp on lightweight metallic substrates: Ab initio and experimental insights, Applied Surface Science **600**, 153947 (2022).
[9] F. Benini, P. Restuccia, and M. C. Righi, Zinc dialkyldithiophosphates adsorption and dissociation on ferrous substrates: An ab initio study, Applied Surface Science **642**, 158419 (2024).
[10] V. R. Salinas Ruiz, T. Kuwahara, J. Galipaud, K. Masenelli-Varlot, M. B. Hassine, C. Héau, M. Stoll, L. Mayrhofer, G. Moras, J. M. Martin, *et al.*, Interplay of mechanics and chemistry governs wear of diamond-like carbon coatings interacting with zddp-additivated lubricants, Nature Communications **12**, 4550 (2021).
[11] N. J. Mosey and T. K. Woo, Insights into the chemical behavior of zinc dialkyldithiophosphate anti-wear additives in their isomeric and decomposed forms through molecular simulation, Tribology international **39**, 979 (2006).
[12] F. Benini, P. Restuccia, E. Pedretti, and M. C. Righi, Ab initio insights into zinc dialkyldithiophosphate linkage isomers and oxidative degradation: Implications for tribology, ACS Applied Nano Materials 10.1021/acsanm.5c01971 (2025).
[13] A. Pacini, M. Ferrario, and M. C. Righi, Accelerating data set population for training machine learning potentials with automated system generation and strategic sampling, Journal of Chemical Theory and Computation https://doi.org/10.1140/epjp/s13360-024-05348-z (2025).
[14] I. Batatia, D. P. Kovacs, G. Simm, C. Ortner, and G. Csányi, Mace: Higher order equivariant message passing neural networks for fast and accurate force fields, Advances in neural information processing systems **35**, 11423 (2022).
[15] I. Batatia, S. Batzner, D. P. Kovács, A. Musaelian, G. N. Simm, R. Drautz, C. Ortner, B. Kozinsky, and G. Csányi, The design space of e (3)-equivariant atom-centred interatomic potentials, Nature Machine Intelligence **7**, 56 (2025).
[16] H. Wang, L. Zhang, J. Han, *et al.*, Deepmd-kit: A deep learning package for many-body potential energy representation and molecular dynamics, Computer Physics Communications **228**, 178 (2018).
[17] A. P. Thompson, H. M. Aktulga, R. Berger, D. S. Bolintineanu, W. M. Brown, P. S. Crozier, P. J. in 't Veld, A. Kohlmeyer, S. G. Moore, T. D. Nguyen, R. Shan, M. J. Stevens, J. Tranchida, C. Trott, and S. J. Plimpton, Lammps - a flexible simulation tool for particle-based materials modeling at the atomic, meso, and continuum scales, Computer Physics Communications **271**, 108171 (2022).
[18] B. Deng, P. Zhong, K. Jun, J. Riebesell, K. Han, C. J. Bartel, and G. Ceder, Chgnet as a pretrained universal neural network potential for charge-informed atomistic modelling, Nature Machine Intelligence **5**, 1031 (2023).
[19] P. Giannozzi, S. Baroni, N. Bonini, M. Calandra, R. Car, C. Cavazzoni, D. Ceresoli, G. L. Chiarotti, M. Cococcioni, I. Dabo, *et al.*, Quantum espresso: a modular and open-source software project for quantum simulations of materials, Journal of Physics: Condensed Matter **21**, 395502 (2009).
[20] P. Giannozzi, O. Andreussi, T. Brumme, O. Bunau, M. B. Nardelli, M. Calandra, R. Car, C. Cavazzoni, D. Ceresoli, M. Cococcioni, *et al.*, Advanced capabilities for materials modelling with quantum espresso, Journal of Physics: Condensed Matter **29**, 465901 (2017).
[21] P. Giannozzi, O. Baseggio, P. Bonfà, D. Brunato, R. Car, I. Carnimeo, C. Cavazzoni, S. D. Gironcoli, P. Delugas, F. F. Ruffino, *et al.*, Quantum espresso toward the exascale, The Journal of Chemical Physics **152**, 154105 (2020).
[22] J. P. Perdew, K. Burke, and M. Ernzerhof, Generalized gradient approximation made simple, Physical Review Letters **77**, 3865 (1996).
[23] S. Grimme, J. Antony, S. Ehrlich, and H. Krieg, A consistent and accurate ab initio parametrization of density functional dispersion correction (dft-d) for the 94 elements h-pu, The Journal of Chemical Physics **132**, 154104 (2010).
[24] I. Batatia, P. Benner, Y. Chiang, A. M. Elena, D. P. Kovács, J. Riebesell, X. R. Advincula, M. Asta, M. Avaylon, W. J. Baldwin, *et al.*, A foundation model for atomistic materials chemistry, arXiv preprint arXiv:2401.00096 https://doi.org/10.48550/arXiv.2401.00096 (2023).
[25] A. D. Kaplan, R. Liu, J. Qi, T. W. Ko, B. Deng, J. Riebesell, G. Ceder, K. A. Persson, and S. P. Ong, A foundational potential energy surface dataset for materials,

arXiv preprint arXiv:2503.04070 (2025).
[26] L. Martínez, R. Andrade, E. G. Birgin, and J. M. Martínez, Packmol: A package for building initial configurations for molecular dynamics simulations, Journal of Computational Chemistry **30**, 2157 (2009), https://onlinelibrary.wiley.com/doi/pdf/10.1002/jcc.21224.
[27] G. Bussi, D. Donadio, and M. Parrinello, Canonical sampling through velocity rescaling, The Journal of chemical physics **126** (2007).
[28] G. Henkelman and H. Jónsson, Improved tangent estimate in the nudged elastic band method for finding minimum energy paths and saddle points, The Journal of chemical physics **113**, 9978 (2000).
[29] Y. Liu, X. He, and Y. Mo, Discrepancies and error evaluation metrics for machine learning interatomic potentials, npj Computational Materials **9**, 174 (2023).
[30] Y. Zuo, C. Chen, X. Li, Z. Deng, Y. Chen, J. Behler, G. Csányi, A. V. Shapeev, A. P. Thompson, M. A. Wood, and S. P. Ong, Performance and cost assessment of machine learning interatomic potentials, The Journal of Physical Chemistry A **124**, 731 (2020).